Bifurcation to 3D Helical Magnetic Equilibrium in an Axisymmetric Toroidal Device

W. F. Bergerson,[1] F. Auriemma,[2] B. E. Chapman,[3] W. X. Ding,[1,4] P. Zanca,[2] D. L. Brower,[1,4] P. Innocente,[2] L. Lin,[1] R. Lorenzini,[2] E. Martines,[2] B. Momo,[2] J. S. Sarff,[3,4] and D. Terranova[2]

[1]*Department of Physics and Astronomy, University of California Los Angeles, Los Angeles, California 90095, USA*
[2]*Consorzio RFX, Associazione EURATOM-ENEA sulla Fusione, 35127 Padova, Italy*
[3]*Department of Physics, University of Wisconsin-Madison, Madison, Wisconsin 53706, USA*
[4]*Center for Magnetic Self-Organization in Astrophysical and Laboratory Plasmas, University of Wisconsin-Madison, Madison, Wisconsin 53706, USA*

(Received 20 June 2011; published 13 December 2011)

We report the first direct measurement of the internal magnetic field structure associated with a 3D helical equilibrium generated spontaneously in the core of an axisymmetric toroidal plasma containment device. Magnetohydrodynamic equilibrium bifurcation occurs in a reversed-field pinch when the innermost resonant magnetic perturbation grows to a large amplitude, reaching up to 8% of the mean field strength. Magnetic topology evolution is determined by measuring the Faraday effect, revealing that, as the perturbation grows, toroidal symmetry is broken and a helical equilibrium is established.

DOI: 10.1103/PhysRevLett.107.255001 PACS numbers: 52.55.Hc, 52.35.Py, 52.55.Fa, 52.55.Tn

There is a rapidly growing appreciation that 3D physics can play a critical role in nominally axisymmetric toroidal magnetic fusion devices such as the tokamak and reversed-field pinch. In such configurations, the toroidal coordinate is usually considered to be ignorable, making the plasma effectively 2D, but there are cases in which toroidal symmetry is broken. One example of this is the emergence in the plasma core of a helical magnetic structure, not unlike the magnetic equilibrium in a stellarator, but produced without the stellarator's set of 3D external field coils. Such a transition to a nonaxisymmetric equilibrium was suggested as a possible explanation for the ''snake'' phenomenon observed in the JET tokamak [1]. Following the injection of a frozen deuterium pellet, a snakelike structure was observed in soft-x-ray emission, and was associated with a magnetic tearing perturbation resonant in the plasma core, with poloidal mode number $m = 1$ and toroidal mode number $n = 1$. A helical magnetic axis was also predicted in the DIII-D tokamak in an examination of sawtooth crash oscillations in oval-shaped plasmas [2]. Well after each sawtooth crash, there was a significant departure from axisymmetry.

Recent computational work on tokamak equilibria characterize plasmas with such a helical structure as a magnetohydrodynamic minimum energy state [3]. This state is accessed through a bifurcation, with the resultant plasma having an internal 3D helical magnetic equilibrium. The helical equilibrium in this case has the same helicity as the experimentally observed perturbation. More recent work has shown that this bifurcation may occur for plasmas expected in the ITER tokamak, presently under construction [4].

Computationally, reversed-field pinch plasmas are also predicted to exhibit a bifurcation to a nonaxisymmetric equilibrium. Topologically, this is referred to as a saddle-node bifurcation, where the axisymmetric axis and the island X point collide, and the separatrix of the island is suppressed [5]. Experimentally, as the toroidal plasma current is increased in RFX-mod, the innermost resonant tearing perturbation grows to large amplitude, saturates, and evolves to an equilibrium with a single helical axis, referred to as SHAx [6]. The 3D nature of this equilibrium has been deduced experimentally through the shapes of the electron temperature and x-ray emission profiles [7], and through magnetic equilibrium reconstruction constrained by measurements of the magnetic field at the plasma boundary [8]. Nonaxisymmetric shaping can serve to enhance confinement properties [6] and greatly expand the design space [9] of toroidal magnetic confinement devices and, consequently, may be of importance for future fusion reactor development.

In this Letter, we report on the first direct measurements of the internal magnetic field structure associated with an emerging 3D helical equilibrium in a magnetically confined toroidal plasma. Axisymmetric Madison Symmetric Torus (MST) [10] reversed-field pinch plasmas undergo a spontaneous self-distortion of the magnetic axis that conforms to the helicity of the dominant, innermost tearing perturbation having mode number ($m = 1$, $n = 5$). The transition is preceded by the growth of this mode and concomitant reduction of the secondary modes ($m = 1$, $n \geq 6$). Interior magnetic topology dynamics are identified using a high-resolution, laser-based diagnostic combining both Faraday rotation and interferometry measurements [11–14], thereby allowing simultaneous detection of the magnetic field and electron density distributions. Before the $n = 5$ perturbation grows to large amplitude and saturates, Faraday rotation time traces indicate that the plasma is toroidally axisymmetric. Then, as the mode begins to grow, signs of topological change become evident, including an asymmetric distortion of the magnetic field that is

largest at the location of the helical structure (former O-point location) in the plasma interior. In these same plasmas, interferometric measurements reveal that the density profile also exhibits an asymmetric structure. A nonaxisymmetric helical equilibrium is computed and compared with both the Faraday rotation and plasma density measurements, providing good spatial and temporal agreement. The magnetic topology is characterized by a 3D helical core surrounded by a 2D axisymmetric plasma shell.

The data presented herein were obtained from MST plasmas having a major radius $R_0 = 1.5$ m and minor radius $a = 0.5$ m. The deuterium plasmas have a maximum toroidal plasma current $I_p \approx 0.6$ MA and a central line-averaged electron density $\bar{n}_e \approx 0.5 \times 10^{19}$ m^{-3}. Tearing perturbations (modes) are driven unstable in these plasmas due to a naturally occurring gradient in the radial profile of the inductively-driven plasma current. This current profile was measured previously with the Faraday rotation diagnostic in toroidally axisymmetric plasmas [12].

The temporal evolution of the lowest-n, $m = 1$ tearing modes in a plasma with spontaneous toroidal symmetry breaking is shown in Fig. 1(a). Fluctuations in the toroidal magnetic field, δb_ϕ, associated with the tearing modes are measured at the plasma boundary with a toroidal array of magnetic sensing coils. Around 18 ms, the $n = 5$ mode begins to grow rapidly, eventually saturating at an amplitude $\delta b^5_\phi(a)/B_\theta(a) \approx 8\%$, where $B_\theta(a)$ is the poloidal field at the plasma boundary. Simultaneously, there is a modest reduction in the modes with $n \geq 6$, leading to a very peaked $m = 1$ mode spectrum with $\delta b^5_\phi / \delta b^{6-9}_\phi > 10$, where the denominator is the square root of the sum of the squares of the $n \geq 6$ mode amplitudes. MST plasmas with a peaked mode spectrum are observed over a range of toroidal plasma

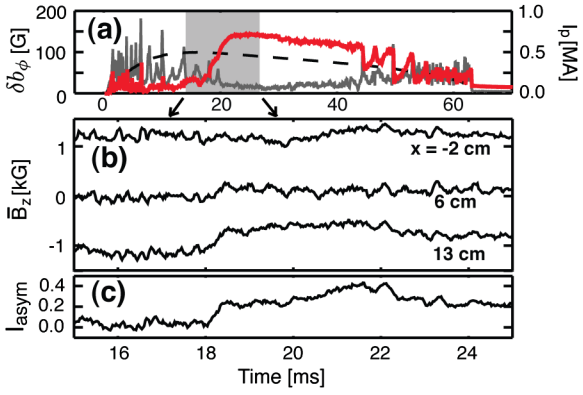

FIG. 1 (color online). Temporal evolution of (a) plasma current I_p (dashed line), the dominant mode δb^5_ϕ (bold-red line), and secondary modes δb^{6-9}_ϕ summed together (grey line), (b) density-weighted line-averaged magnetic field, $\bar{B}_z(t)$, at impact parameters $= -2$, 6, and 13 cm, and (c) asymmetry factor (defined in text) during the transition to helical state. Data from shot 1110915006.

current, but the dominant mode achieves its largest amplitude at the largest current.

The temporal dynamics of internal magnetic and density structures are measured by a high-speed, high-precision, laser-based, polarimeter-interferometer system which has 11 chords (spacing $\Delta x \sim 7$–8 cm) across the plasma diameter [11]. The chords are arranged in two sets, one set (6 chords) displaced five degrees toroidally from the other. Along each chord the system measures simultaneously the equilibrium and fluctuating values of the line-integrated density, $\phi(x) = c_i \int n_e dz$, and the Faraday rotation effect, $\psi(x) = c_F \int n_e B_z dz$, where c_i and c_F are constants, $x = R - R_0$ is the impact parameter, and dz is the chord length [14]. The density-weighted line-averaged magnetic field $\bar{B}_z = \int n_e B_z dz / \int n_e dz$ for the three central-most chords is shown in Fig. 1(b) at times before, during, and after the growth of the $n = 5$ mode. Before 18 ms, there is no mean magnetic field component, B_z, along the chord at $x = +6$ cm because it is perpendicular to the toroidal and poloidal fields. Also during this time, the chords at $x = -2$ and $+13$ cm (inboard and outboard) have the same magnitude because they are tangent to the same core flux surface. The opposite sign results from the component of the poloidal magnetic field parallel to the laser beam changing direction across the magnetic axis. For chords with impact parameter near the magnetic axis, the measurements are spatially localized to the plasma core as the only contribution to the line-integrated measurement occurs there [12,13].

As the $n = 5$ mode amplitude begins to grow ($t \sim 18$ ms), $\bar{B}_z$ along the outboard chord changes significantly, while there is little or no change in $\bar{B}_z$ along the inboard chord as shown in Fig. 1(b). Furthermore, $\bar{B}_z$ along the chord at $x = +6$ cm now deviates from zero, implying a prompt displacement of the core current channel within $\sim$0.5 ms. To quantify this difference in magnetic field change between the inboard and outboard chords, we define an asymmetry factor $I_{\text{asym}} = [|\bar{B}_z(+)| - |\bar{B}_z(-)|]/B_\theta(a)$, where $+/-$ refers to the inboard/outboard chord locations. Note that $I_{\text{asym}} = 0$ reflects perfect symmetry, and contributions to I_{asym} from the equilibrium Shafranov shift are negligible for the central chords being discussed. As shown in Fig. 1(c), the asymmetry factor remains near zero before 18 ms but reaches nearly 0.4 shortly after, indicating significant deviation from axisymmetry. Measurement uncertainty in I_{asym} is $\sim$0.1. Symmetry breaking can be caused by helical deformation associated with a single tearing mode or a helical current. For example, the perturbation from an $m = 1$ tearing mode on $\bar{B}_z(+)$ and $\bar{B}_z(-)$ is nearly the same [i.e., $\Delta B_z(+) \cong \Delta B_z(-)$, where Δ denotes the change of magnetic field during the transition from multiple helicity, $t < 18$ ms, to single helicity, $t > 18$ ms] because of opposing perturbing currents in the O and X points leading to $I_{\text{asym}} \neq 0$ [13]. However, measurements show that after $t = 18$ ms, the

change in the magnetic field inboard, $\Delta\bar{B}_z(x = -2\ \mathrm{cm}) < 50$ G, is markedly different from the change in the magnetic field outboard, $\Delta\bar{B}_z(x = +13\ \mathrm{cm})$ up to 530 G, thereby implying a diminished fluctuating current near the X point. This result is inconsistent with routinely observed $m = 1$ tearing modes and provides experimental evidence for a distortion of the magnetic topology into a 3D helical equilibrium.

The measurements presented in Fig. 1 reflect directly the breaking of symmetry in the plasma core. The growth to large amplitude of the $n = 5$ mode generates an electromagnetic braking torque which causes the mode's normally rapid rotation to slow and eventually cease, or lock [15]. In the discharge in Fig. 1, the $n = 5$ structure comes to rest shortly after 18 ms along the outboard midplane at the location of the Faraday rotation diagnostic and is intersected by the $x = +13$ cm chord. The locking orientation of the $n = 5$ structure varies from shot to shot. When, for example, the $n = 5$ structure locks inboard of the magnetic axis, the largest magnetic field distortion is observed along the $x = -2$ cm chord, and the asymmetry factor changes sign, becoming negative.

The breaking of axisymmetry is also observed through interferometric measurement of the density distribution. Profiles of the line-integrated density from three different plasmas, with $I_{\mathrm{asym}} \approx -0.4$, 0.4, and 0, are shown in Fig. 2. Plasmas with $I_{\mathrm{asym}} \approx \pm 0.4$ are similar to data shown in Fig. 1. Changes in the density profile are observable when $|I_{\mathrm{asym}}| > 0.1$. For the outboard case, where $I_{\mathrm{asym}} > 0$, the line-integrated density in the outboard chords is larger than that for the axisymmetric profile, while the line-integrated density along the inboard chords is smaller. For the inboard case, where $I_{\mathrm{asym}} < 0$, the opposite is true. Calculation of the density profile centroid location is one means of quantifying the difference between these two asymmetric profiles. The location of the density profile centroid is defined as $\bar{x} = \sum x\phi(x)/\sum \phi(x)$. For the standard axisymmetric equilibrium, $\bar{x} = +4.0$ cm, the result of an outward Shafranov shift. For the outboard case, $\bar{x} = +5.6$ cm, while for the inboard case, $\bar{x} = +1.9$ cm, both reflecting a centroid shift of about 2 cm relative to the axisymmetric case. The measured density profile suggests that there is a nonaxisymmetric equilibrium in the core.

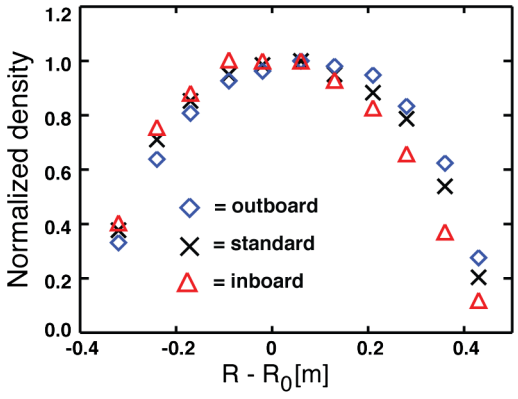

FIG. 2 (color online). Measured profiles of the line-integrated density for $I_{\mathrm{asym}} < 0$ (inboard, red triangles, shot 1100914044) and $I_{\mathrm{asym}} > 0$ (outboard, blue diamonds, shot 1100915071), and $I_{\mathrm{asym}} \approx 0$ (standard axisymmetric density, black X, shot 1100915071). Density measurements have been normalized to the value at $R - R_0 = 0.06$ m. Error bars are comparable to symbol size.

To better visualize the 3D nature of these MST plasmas, we reconstruct the magnetic topology based on measurements at the plasma boundary of the equilibrium and fluctuating magnetic fields. The reconstruction is then compared, successfully, with the internal constraints provided by Faraday rotation and interferometry measurements. The nonaxisymmetric reconstruction technique used is a variant [16] of that developed for similar plasmas in RFX-mod [8]. The axisymmetric portion of the magnetic equilibrium is calculated with a model based on a toroidal geometry. The nonaxisymmetric helical distortion due to the eigenfunction of the innermost resonant mode is calculated via Newcomb's equation, again in toroidal geometry. The composite equilibrium is shown in Fig. 3(a). This reconstruction corresponds to a case in which the O point of the original helical perturbation locks in an outboard orientation at the location of the Faraday rotation diagnostic, as was the case for the discharge in Fig. 1. There are two key features to note in this figure. First, there is only one magnetic axis, located far off the geometric center −− the original Shafranov-shifted magnetic axis of the toroidal axisymmetric equilibrium has disappeared. Second, the magnetic topology consists of a helical core surrounded by an axisymmetric outer shell, the latter being enforced by the axisymmetric conducting shell at the plasma boundary.

Once the 3D flux surface geometry is determined, it can serve as the basis upon which to invert the line-integrated density measurements and determine the local density everywhere in space by application of a minimization process [16]. The reconstructed density profile is shown

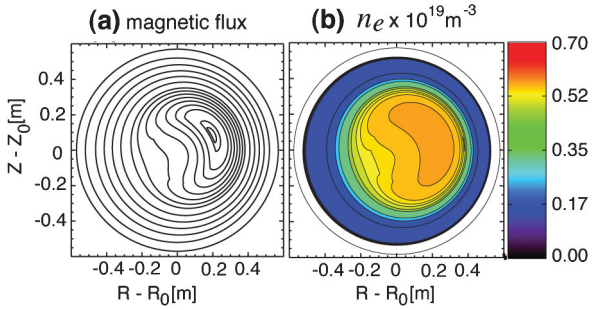

FIG. 3 (color). (a) Magnetic flux surfaces as determined by the helical reconstruction code, (b) reconstruction of local density resulting from fit to the nonaxisymmetric helical flux surfaces. Data taken from shot 1100915018.

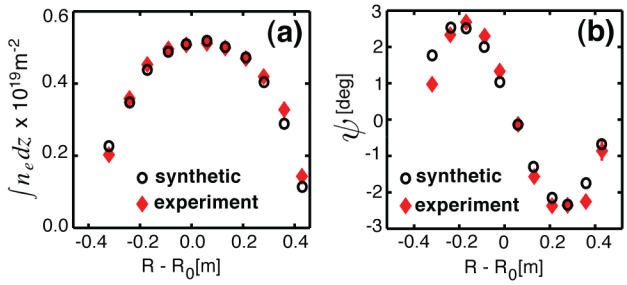

FIG. 4 (color online). Comparison of measured (solid red diamonds) to synthetic diagnostic (open black circles) from reconstruction for line-integrated (a) density and (b) Faraday rotation profiles. Data taken from shot 1100915018. Line-integrated profiles are based on the same data as shown in Fig. 3. Error bars are comparable to symbol size.

in Fig. 3(b). Like the equilibrium flux surfaces, the equilibrium density exhibits a helical bean structure in the core with an axisymmetric boundary. It is clear that the flux surface and density profile reconstructions are topologically similar. This outcome is enforced by the inversion process where the density is held constant on each flux surface.

Both the density and magnetic field profile reconstructions have been benchmarked against the experimental measurements. In Fig. 4(a), line-integrated density profiles from measurement and computation based on the helical inversion are shown to be in excellent agreement. A more robust test of the helical reconstruction probes its ability to reproduce accurately the Faraday rotation data that comprise the $\bar{B}_z$ data shown earlier. By combining the two reconstructed profiles in Fig. 3, and adding a synthetic Faraday rotation diagnostic, one can compare directly the experimentally measured line integrals to that in the reconstruction. This is a more rigorous test since the magnetic reconstruction was not constrained by the experimental Faraday rotation data. The comparison of experimental and synthetic data is shown in Fig. 4(b), where good agreement between the two is observed. The χ^2 fit improves 50% when utilizing a helical basis rather than the toroidal axisymmetric model for the density and Faraday reconstructions. In synthesizing the density and Faraday rotation data, toroidal displacement of the two sets of offset chords must be included. The poloidal location of the $n = 5$ helical structure rotates 25° between the two sets, consistent with measurements.

Beyond its ability to match the Faraday rotation data at a single point in time, the reconstruction code can also track the temporal dynamics of the helical equilibrium evolution. To illustrate, the reconstruction is used to track the location in the plasma core where the Faraday rotation effect $\bar{B}_z = 0$. The experimentally measured time evolution of this zero-crossing (obtained from linear interpolation between the $x = -2$ and $+13$ cm chords) for a single MST discharge is plotted as a solid line in Fig. 5. This again

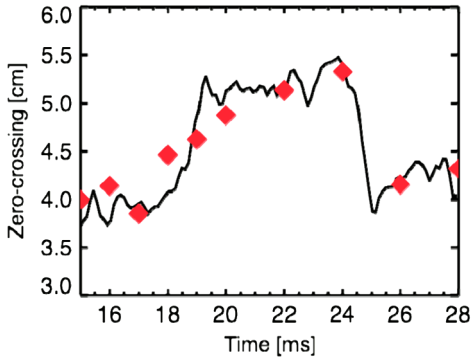

FIG. 5 (color online). Measured Faraday rotation zero-crossing (solid line) compared to 3D reconstruction (red diamonds) for MST plasma with spontaneous transition into and out of a helical core. Helical structure is located near the outboard midplane. Data taken from shot 1100915079.

is a case where the helical structure is outboard at the location of the Faraday rotation diagnostic. Overplotted in this figure are red diamonds showing the reconstructed (predicted) zero-crossing locations, this time from a temporal series of helical reconstructions. The displacement of the measured zero-crossing is well reproduced by the nonaxisymmetric reconstructions both for the transition into the 3D helical equilibrium as well as the back transition at ~25 ms.

In this Letter we have demonstrated for the first time the direct measurement and characterization of the core magnetic field associated with the bifurcation of a 2D toroidally axisymmetric plasma into a 3D topology with broken toroidal symmetry. As the innermost resonant $m = 1$ tearing mode grows to large amplitude and saturates, the initially small helical perturbation evolves into a new, helical equilibrium. This equilibrium is observed directly as a substantial asymmetric distortion of the line-integrated magnetic field and electron density. Reconstruction of the helical equilibrium is found to agree well, both spatially and temporally, with the direct internal measurements. By combining the internal measurements with the nonaxisymmetric equilibrium reconstruction, we can proceed in the future to more accurately identify the internal dynamics and confinement properties of the 3D equilibrium.

[1] A. Weller *et al.*, Phys. Rev. Lett. **59**, 2303 (1987).
[2] E. A. Lazarus *et al.*, Plasma Phys. Controlled Fusion **48**, L65 (2006).
[3] W. A. Cooper *et al.*, Phys. Rev. Lett. **105**, 035003 (2010).
[4] W. A. Cooper, J. P. Graves, and O. Sauter, Plasma Phys. Controlled Fusion **53**, 024002 (2011).
[5] D. F. Escande *et al.*, Phys. Rev. Lett. **85**, 3169 (2000).
[6] R. Lorenzini *et al.*, Phys. Rev. Lett. **101**, 025005 (2008).
[7] R. Lorenzini *et al.*, Phys. Plasmas **16**, 056109 (2009).

[8] E. Martines *et al.*, Plasma Phys. Controlled Fusion **53**, 035015 (2011).
[9] A. H. Boozer, Phys. Plasmas **16**, 058102 (2009).
[10] R. N. Dexter *et al.*, Fusion Technol. **19**, 131 (1991).
[11] W. X. Ding *et al.*, Rev. Sci. Instrum. **75**, 3387 (2004).
[12] D. L. Brower *et al.*, Phys. Rev. Lett. **88**, 185005 (2002).
[13] W. X. Ding *et al.*, Phys. Rev. Lett. **90**, 035002 (2003).
[14] D. L. Brower *et al.*, Rev. Sci. Instrum. **74**, 1534 (2003).
[15] B. E. Chapman *et al.*, Phys. Plasmas **11**, 2156 (2004).
[16] F. Auriemma *et al.*, Plasma Phys. Controlled Fusion **53**, 105006 (2011).